

Fast Neutrino Flavor Conversions Can Help and Hinder Neutrino-Driven Explosions

Jakob Ehring^{1,2,3}, Sajad Abbar¹, Hans-Thomas Janka², Georg Raffelt¹, and Irene Tamborra⁴

¹Max-Planck-Institut für Physik (Werner-Heisenberg-Institut), Föhringer Ring 6, D-80805 München, Germany

²Max-Planck-Institut für Astrophysik, Karl-Schwarzschild-Straße 1, D-85748 Garching, Germany

³Technical University of Munich, TUM School of Natural Sciences, Physics Department,

James-Frank-Straße 1, D-85748 Garching, Germany

⁴Niels Bohr International Academy & DARK, Niels Bohr Institute, University of Copenhagen,

Blegdamsvej 17, DK-2100 Copenhagen, Denmark



(Received 22 May 2023; accepted 17 July 2023; published 7 August 2023)

We present the first simulations of core-collapse supernovae in axial symmetry with feedback from fast neutrino flavor conversion (FFC). Our schematic treatment of FFCs assumes instantaneous flavor equilibration under the constraint of lepton-number conservation individually for each flavor. Systematically varying the spatial domain where FFCs are assumed to occur, we find that they facilitate SN explosions in low-mass (9–12 M_{\odot}) progenitors that otherwise explode with longer time delays, whereas FFCs weaken the tendency to explode of higher-mass (around 20 M_{\odot}) progenitors.

DOI: [10.1103/PhysRevLett.131.061401](https://doi.org/10.1103/PhysRevLett.131.061401)

Introduction and motivation.—Multidimensional simulations of core-collapse supernovae (CCSNe) with refined, energy-dependent neutrino transport, in particular also in three dimensions (3D), support the viability of the neutrino-driven explosion mechanism [1–8]. Since the huge binding energy of several 10^{53} erg of a newly formed protoneutron star (PNS) is carried away by neutrinos and antineutrinos of all flavors, about one percent of this energy is well sufficient to explain the vast majority of the observed CCSNe [9]. The energy transfer to the explosion is mostly mediated by the absorption of several percent of the escaping electron (anti)neutrinos (ν_e and $\bar{\nu}_e$) on free neutrons and protons behind the stalled core-bounce shock [10]. These reactions therefore decide about success or failure of the explosion. They also determine the neutron-to-proton ratio and thus the formation of chemical elements in the innermost ejecta of successful explosions. Neutrinos of other flavors (commonly pooled as ν_x) do not interact via charged-current processes in the ejected matter and thus are subdominant for powering the explosion, although their creation by thermal pair processes contributes significantly to PNS cooling. For numerical models to be predictive, and to understand the processes that trigger and power the blast wave, a reliable implementation of neutrino transport and flavor evolution in the deep SN interior is indispensable [11–15].

Neutrino flavor conversions in the SN core remain one of the major uncertainties for rigorous, self-consistent *ab initio* modeling. Despite the long-standing insight that neutrinos can change flavor during propagation, the possible consequences have usually been ignored in SN simulations. But the extremely high neutrino number densities in this environment facilitate nonlinear, collective phenomena that are not suppressed by matter effects [16]. In particular, ν and $\bar{\nu}$ can pairwise undergo so-called fast flavor conversions (FFCs) [17–22]. The characteristic length scales depend on the neutrino number density and can be as short as centimeters. FFCs have been at the focus of numerous recent investigations, and their possible occurrence has been diagnosed in different regions inside the PNS, in the neutrino-decoupling layer, and ahead and behind the SN shock [23–28].

Here, we explore, for the first time, the impact of FFCs on the evolution of collapsing stars by multidimensional neutrino-hydrodynamic simulations, thus expanding our previous work in spherical symmetry [29]. Considering several, distinctly different progenitor models, we demonstrate that the consequences of FFCs depend on the stellar core structure and mass range. The quantum kinetic problem of neutrino flavor transport still awaits a practical solution. Therefore, once more we apply our schematic treatment [29], i.e., we assume that below a chosen critical density ρ_c , FFCs lead to flavor equilibrium under the constraint of lepton-number conservation (thus maximizing the impact of FFCs).

Interestingly, our results show that FFCs can both support or suppress neutrino-driven explosions, with the exact dynamical response depending on the progenitor and the assumed region of flavor conversions.

Published by the American Physical Society under the terms of the [Creative Commons Attribution 4.0 International](https://creativecommons.org/licenses/by/4.0/) license. Further distribution of this work must maintain attribution to the author(s) and the published article's title, journal citation, and DOI. Open access publication funded by the Max Planck Society.

Numerical setup and set of simulations.—Our simulations were performed in axial symmetry (2D) with the neutrino-hydrodynamics code *ALCAR* [30,31]. This is a state-of-the-art, Eulerian, conservative, higher-order Godunov-type finite-volume solver for the 1D and multi-D fluid dynamics equations coupled to a two-moment scheme for energy-dependent three-flavor neutrino transport. It uses a well-tested implementation of all relevant neutrino processes. The main features, input physics, numerical setup of the models, and description of the FFC implementation are provided in our earlier paper [29].

In the absence of a fundamental prescription, and to enable a systematic parametric study, we assume that FFCs take place in the entire volume where $\rho < \rho_c$, a chosen density threshold value. We assume that pairwise $\nu\bar{\nu}$ flavor conversion is “instantaneous,” i.e., on length scales much less than our numerical cells and timescales defined by our computational time stepping. This approach is justified for FFCs (and any other flavor conversion phenomenon) that proceed on scales much below the resolution of full-scale hydrodynamic CCSN models. We further assume that FFCs lead to complete flavor equilibrium under the constraints of lepton number conservation for each flavor individually, in particular also of electron-neutrino lepton number, as well as energy and total momentum conservation, and with respecting the Pauli exclusion principle. Our algorithm, defined in Eqs. (9), (10), (14), and (15) of Ref. [29], is applied after each time step in each spatial cell

where $\rho < \rho_c$. Some recent studies have focused on the asymptotic FFC state [32]. We stress that our recipe leads to a converged state: it does not change if the algorithm is applied twice.

Our simulations were evolved in 1D until 5 ms pb (post bounce) and then mapped onto a 2D polar coordinate grid consisting of 640 logarithmically spaced radial zones and 80 equidistant lateral ones. The central 2 km core was still calculated in 1D, permitting larger time steps, yet having negligible influence on the hydrodynamic evolution. During the mapping, random cell-by-cell perturbations of 0.1% of the local density were applied to seed the hydrodynamic instabilities, which otherwise would develop only due to uncontrolled numerical noise.

We selected three progenitors with different zero-age main-sequence masses. One is the $20M_\odot$ model [33] that we used in our previous 1D study [29]. In addition, we investigated a $9M_\odot$ [34] and $11.2M_\odot$ model [35]. The $9M_\odot$ star consistently explodes in multi-D simulations, although in some more quickly and about twice as energetically [6,8,36] than in others [31,37,38]. The $11.2M_\odot$ model is less ready to blow up, exhibiting a delayed and slow onset of shock expansion [39–42]. In contrast, the $20M_\odot$ star failed to explode in most multi-D simulations [31,37,43,44].

The convention for naming our simulations follows our previous one [29], supplemented with a numerical value for the stellar mass: $M9.0$ -2D-xxx, $M11.2$ -2D-xxx, and $M20.0$ -2D-xxx. Here, xxx is a placeholder for either noFC

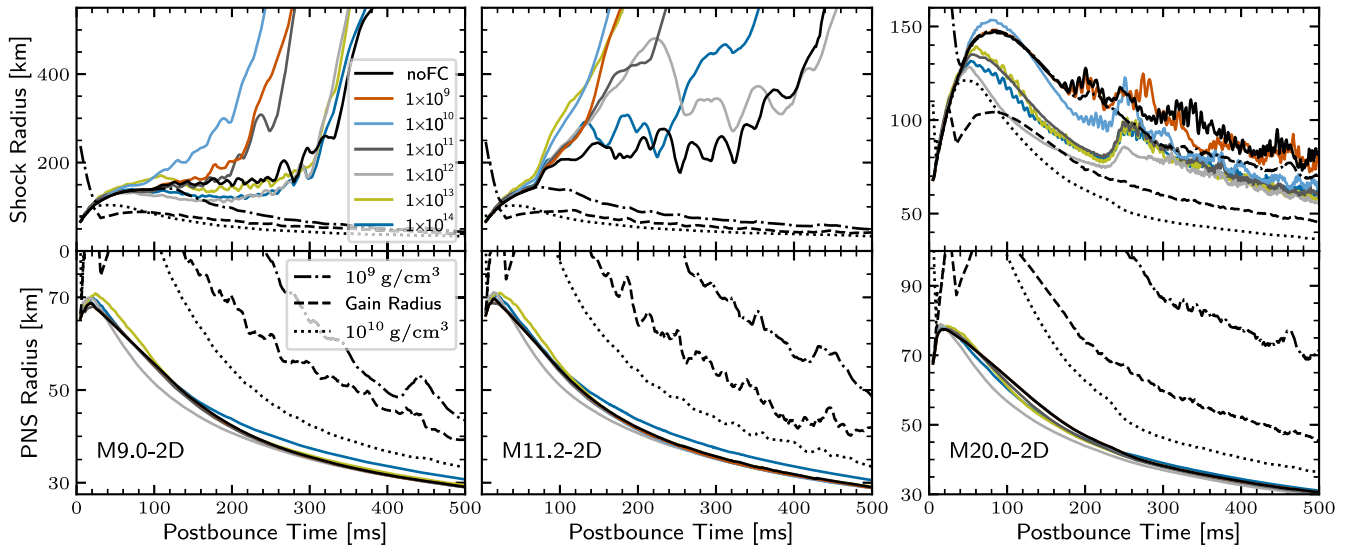


FIG. 1. Angle-averaged shock radii (top) and PNS radii (bottom; defined at $\rho = 10^{11} \text{ g cm}^{-3}$) vs postbounce time for the indicated models. Black solid lines: Models noFC (no flavor conversions). Colored solid lines: Instantaneous FFCs for $\rho < \rho_c$ as labeled in the legend. The unsteady motion of the average shocks with contraction and expansion phases is caused by the violent large-scale convective mass flows in the neutrino heated gain layer behind the CCSN shock. The sudden growth of r_{shock} (small at ~ 100 ms for $M9.0$ -2D and prominent at ~ 70 ms for $M11.2$ -2D and at ~ 220 ms for $M20.0$ -2D) signals a decrease of mass accretion rate due to the arrival of the Si/O interface. For the noFC models, we also show the angle-averaged gain radius (dashed black) and the mean radii for $\rho = 10^9$ and $10^{10} \text{ g cm}^{-3}$ (dash-dotted and dotted black lines, respectively), all smoothed with 10 ms running averages. For the 9.0 and $11.2M_\odot$ progenitors, FFCs support an earlier onset of the explosion, whereas for $20.0M_\odot$ they thwart it and the shock recedes even more rapidly.

(“no flavor conversion”) or for the FFC threshold density. We implement $\rho_c = 10^9 \text{ g cm}^{-3}, \dots, 10^{14} \text{ g cm}^{-3}$ in steps of factors of 10, corresponding to $\text{xxx} = 1e09, \dots, 1e14$.

Results.—In our previous 1D simulations [29] of the $20M_\odot$ progenitor we found that FFCs caused a faster and stronger shock contraction than without FFCs for all threshold densities ρ_c and for all times (except for $\rho_c = 10^{10} \text{ g cm}^{-3}$ during a short period of about 70 ms around 100 ms pb). This finding suggested that FFCs tend to hinder shock revival and neutrino-driven explosions, and this conclusion is confirmed in 2D for the $20M_\odot$ star (Fig. 1).

However, our 9 and $11.2M_\odot$ progenitors demonstrate that this is not generally the case (Fig. 1). Including FFCs, in particular for $\rho_c = 10^9, 10^{10}, 10^{11} \text{ g cm}^{-3}$, yields significantly earlier explosions. The main explanation is a higher net heating rate per nucleon (q_{gain}) for at least ~ 100 ms pb. The increased q_{gain} causes a persistently higher mass M_{gain} in the energy-gain layer behind the stalled shock and a correspondingly higher total net heating rate Q_{gain} in this volume (Fig. 2).

This enhanced heating can be traced to $\nu_x \rightarrow \nu_e, \bar{\nu}_e$ conversions of high-energy heavy-lepton neutrinos exterior to the neutrinospheres. Although the ν_e and $\bar{\nu}_e$ number fluxes exceed the ν_x ones during the accretion phase before the onset of the explosion, equilibration with the more energetic ν_x raises the mean ν_e and $\bar{\nu}_e$ energies, $\langle \epsilon_{\nu_e} \rangle$ and $\langle \epsilon_{\bar{\nu}_e} \rangle$ (Fig. 3, right). Despite the concomitant decrease of the ν_e and $\bar{\nu}_e$ luminosities (Fig. 3, left), the energy transfer to the postshock layer is boosted because $q_{\text{gain}} \propto \langle \epsilon_{\bar{\nu}_e}^2 \rangle$.

The set of simulations $M9.0\text{-}2\text{D-}1e09, 10, 11$ as well as $M11.2\text{-}2\text{D-}1e09, 10, 11$ each exhibit a similarly fast expansion of their shock trajectories. In particular, even the $\rho_c = 10^9 \text{ g cm}^{-3}$ cases feature such a rapid shock revival because the surface of constant $\rho = 10^9 \text{ g cm}^{-3}$ moves behind the shock (Fig. 1, dash-dotted black lines). Therefore $\nu_x \rightarrow \nu_e, \bar{\nu}_e$ conversions take place in a major part of the gain layer even for this low conversion density.

The FFC impact on the postbounce evolution changes when flavor equilibration occurs deeper inside. In $M9.0\text{-}2\text{D-}1e12$ and $M11.2\text{-}2\text{D-}1e12$, the explosion sets in at nearly the same time as without FFC, although the shock transiently expands to nearly 500 km at ~ 220 ms pb in $M11.2\text{-}2\text{D-}1e12$. The subsequent breakdown of the shock expansion follows from extremely rapid PNS contraction (Fig. 1), caused by enhanced cooling due to $\nu_e, \bar{\nu}_e \rightarrow \nu_x$ conversions in the layer between 10^{11} and $10^{12} \text{ g cm}^{-3}$. The ν_x can easily escape from this region exterior to their neutrinosphere. The corresponding luminosities increase visibly in Fig. 3 not only for ν_x , but also for $\bar{\nu}_e$ (and slightly for ν_e) because of the compression heating of their neutrinospheres. This fast PNS contraction also pulls matter from the gain layer into the cooling layer, whose mass is lower than in the quickly exploding model

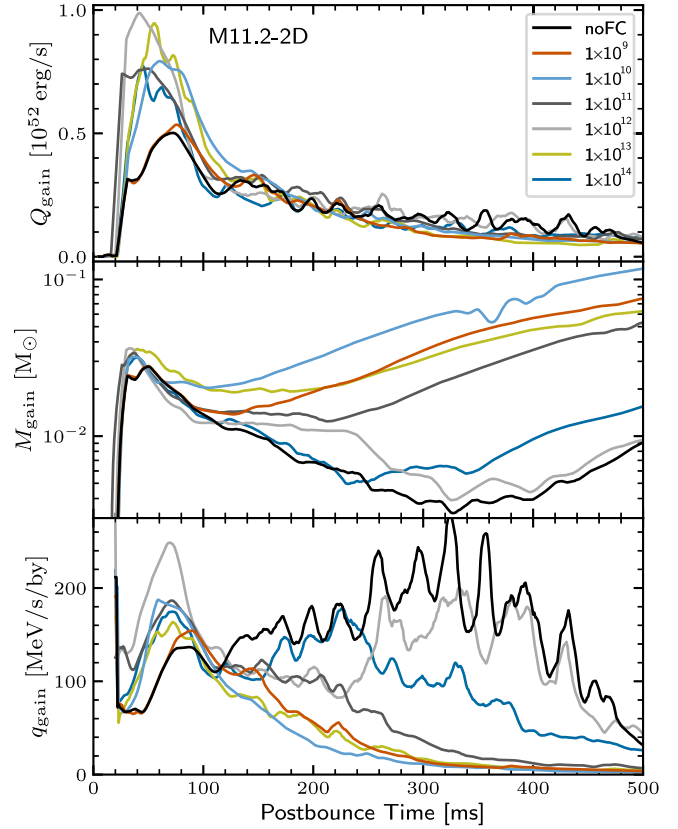


FIG. 2. Total net neutrino-heating rate (top), mass in the gain layer (middle), and net heating rate per baryon (bottom) for our $M11.2\text{-}2\text{D}$ simulations. (10 ms running average.)

$M11.2\text{-}2\text{D-}1e11$ at all times. After ~ 250 ms, q_{gain} , M_{gain} , and Q_{gain} of $M11.2\text{-}2\text{D-}1e12$ become similar to noFC (Fig. 2), for which reason both models ultimately explode in a synchronous way. Similar arguments linked to the faster PNS contraction also apply for $M9.0\text{-}2\text{D-}1e12$.

In $M11.2\text{-}2\text{D-}1e14$, q_{gain} and Q_{gain} before ~ 100 ms are higher than in $M11.2\text{-}2\text{D-noFC}$, but stronger cooling between the gain radius r_{gain} and PNS radius r_{PNS} (at $10^{11} \text{ g cm}^{-3}$) prevents a fast explosion of this model. After ~ 100 ms heating and cooling in the gain and cooling layers and M_{gain} differ little between the two models (Fig. 2). Therefore $M11.2\text{-}2\text{D-}1e14$ explodes only slightly earlier, possibly triggered by stochastically intensified postshock convection. $M9.0\text{-}2\text{D-}1e13$ and 14 compared to noFC show amplified cooling below r_{gain} for roughly 150 ms, and smaller M_{gain} and Q_{gain} from this time until twice longer. In all of these models, including $M9.0\text{-}2\text{D-}1e12$, the explosion sets in only later than ~ 300 ms (Fig. 1).

$M11.2\text{-}2\text{D-}1e13$ is a stark outlier: it sports rapid shock expansion very early and similar to $M11.2\text{-}2\text{D-}1e10$, but in clear contrast to $M9.0\text{-}2\text{D-}1e13$. The favorable explosion conditions in $M11.2\text{-}2\text{D-}1e13$ derive from r_{PNS} exceeding that of any other simulation of this star during the first 100 ms (Fig. 1). This permits more mass to stay in the gain

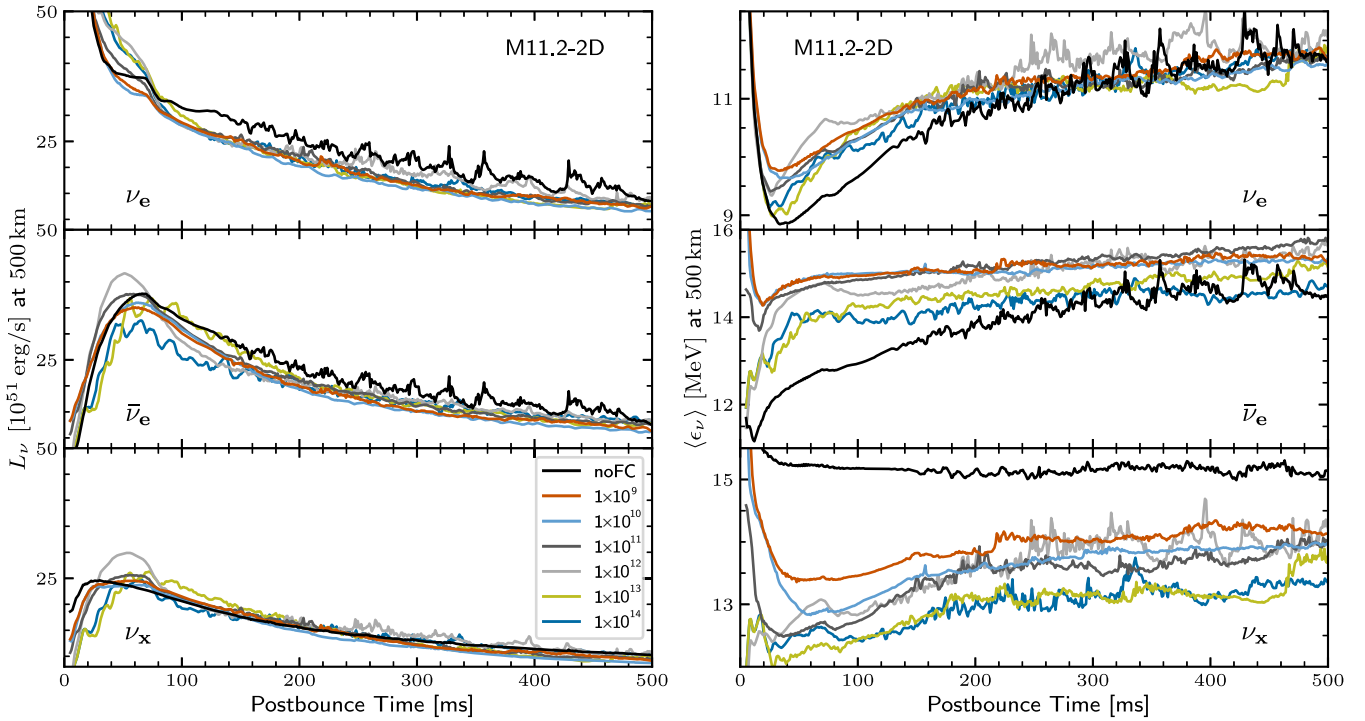


FIG. 3. Evolution of luminosities and mean energies of the radiated ν_e , $\bar{\nu}_e$, and one species of ν_x for our $M11.2$ -2D simulations. All quantities are angle averaged, measured at a radius of 500 km, and transformed to a distant observer at rest.

layer during this period when q_{gain} is enhanced by FFC effects (Fig. 2). These conditions facilitate the runaway shock expansion when the composition interface between the progenitor's Si shell and Si-enriched O shell reaches the shock at $t_{\text{pb}} \sim 70$ ms. The larger r_{PNS} is caused by very strong PNS convection, which is boosted by local heating around $\rho_c = 10^{13} \text{ g cm}^{-3}$. This happens when ν_x diffusing out from the PNS core are converted to ν_e and $\bar{\nu}_e$ just below this threshold density and the newly created ν_e and $\bar{\nu}_e$ get rapidly absorbed in the local medium (see [29] for a detailed description of this effect in 1D). This intriguing convective boost is much weaker when $\nu_x \rightarrow \nu_e, \bar{\nu}_e$ happens at $\rho_c = 10^{14} \text{ g cm}^{-3}$.

This FFC effect on PNS convection and increased r_{PNS} also appears in $M9.0$ -2D-1e13 (Fig. 1). However, in this model the mass accretion rate \dot{M} decreases gradually and a pronounced decline of the density and thus of the mass accretion rate at the progenitor's Si/O interface are absent (Fig. 4). \dot{M} in the $9.0M_{\odot}$ star drops below the one in $11.2M_{\odot}$ only at $t_{\text{pb}} \sim 200$ ms. At this time, q_{gain} , M_{gain} , and Q_{gain} of $M9.0$ -2D-1e13 have come close to noFC and therefore both models exhibit a very similar later shock evolution.

Our findings are completely different for the $20M_{\odot}$ progenitor, where FFCs do not improve the explosion conditions. Without FFCs, there is no explosion within 500 ms pb, and in all FFC cases, the average r_{shock} is even smaller most of the time, with only a few short inversions

(Fig. 1). The overall shock evolution resembles our 1D simulations [29], except for some secondary differences of the PNS contraction and a corresponding reaction of the shock due to the FFC-induced boosting of the PNS convection in $M20.0$ -2D-1e13 and 14. All models fail to explode, because at the time (~ 230 ms) when the Si/O composition interface arrives at the shock, q_{gain} , M_{gain} , and r_{shock} in $M20.0$ -2D-1e09 are close to noFC and in all other FFC models considerably lower.

In this critical phase, the weaker FFC-implied q_{gain} is traced to the high mass infall rate in the collapsing $20M_{\odot}$ star. This leads to the formation of a very massive PNS ($\sim 1.9M_{\odot}$ instead of 1.30 – $1.36M_{\odot}$ in the lower-mass progenitors) that accumulates a hot accretion mantle. As this PNS contracts, $\langle \epsilon_{\nu_e} \rangle$ and $\langle \epsilon_{\bar{\nu}_e} \rangle$ increase quickly in

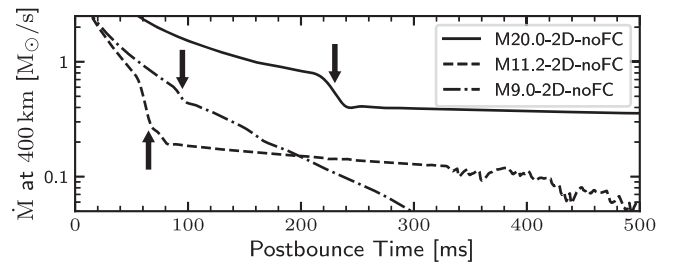


FIG. 4. Mass accretion rates at 400 km for the noFC models. The steplike features (arrows) derive from density jumps at the Si/O interfaces of the collapsing progenitors.

$M20.0\text{-}2\text{D}\text{-noFC}$, whereas $\langle\epsilon_{\nu_x}\rangle$ remains nearly constant. Therefore, $\nu_x \rightarrow \nu_e, \bar{\nu}_e$ can result in only moderately higher $\langle\epsilon_{\nu_e}\rangle$ and $\langle\epsilon_{\bar{\nu}_e}\rangle$. In q_{gain} , these marginally higher $\langle\epsilon_{\nu_e}\rangle$ and $\langle\epsilon_{\bar{\nu}_e}\rangle$ cannot compensate for the considerable reduction of the ν_e and $\bar{\nu}_e$ luminosities caused by flavor equilibration.

Whether FFCs help or hinder the CCSN explosion is therefore tightly connected to \dot{M} and the corresponding growth of the PNS mass and $\langle\epsilon_{\nu}\rangle$ of the radiated neutrinos. This suggests that the dynamical impact of FFCs correlates with the compactness defined in Ref. [45] for characterizing the stellar core structure.

Discussion.—We have studied the possible impact of FFCs on CCSNe by 2D simulations, using a schematic treatment that enforces instantaneous (i.e., on subgrid scales) flavor equilibration under the constraints of energy, momentum, and individual lepton number conservation. We have systematically varied the threshold density below which FFCs are assumed to occur.

Our results suggest that FFCs can both facilitate or weaken the onset of runaway shock expansion, depending on the core structure of the stellar progenitor and the region where FFCs are assumed to occur. Concerning their supportive influence on explosions, FFCs are on a par with a variety of other effects that assist the neutrino-driven mechanism. In particular the 3D nature of precollapse stars in terms of density and velocity perturbations associated with convective oxygen and silicon shell burning is important for the successful shock revival in 3D simulations [46,47]. Neutrino-powered explosions are also fostered by other effects such as muons in the high-density medium [47,48], strangeness-dependent contributions to the axial-vector coupling constant of neutral current neutrino-nucleon scattering [43,49], a higher effective nucleon mass at densities above roughly 10% of the nuclear saturation density [50,51], or magnetic fields. The B fields can aid the initiation of the shock expansion even without the field-amplifying effects of rapid rotation, provided the precollapse core of the progenitor star is strongly magnetized [52–55].

Also, nonstandard physics such as a hadron-quark phase transition [56], beyond-standard-model particle physics [57,58], and modified theories of gravity [59] have been suggested as potentially supportive to shock revival. In contrast to such possibilities, which reach beyond the limits of currently well constrained physics, FFC is a phenomenon that occurs within the framework of well established theory, and its consequences for CCSNe should therefore be better understood.

Further work on practical solutions of the neutrino quantum kinetic equations in SNe and neutron star (NS) mergers is therefore imperative [60]. And simulations for a wider range of progenitors and longer evolution times are needed to explore the consequences of FFCs on observable signals and CCSN properties, for example explosion energies, nucleosynthesis in neutrino-heated ejecta, neutrino

signals from all evolution phases, and gravitational waves, which could be amplified by stronger PNS convection.

In contrast to most of the other effects mentioned above, we found the impact of FFCs on the CCSN dynamics to differ in low-mass and high-mass progenitors. This is an intriguing result and therefore requires verification by more elaborate treatments of the neutrino flavor evolution to replace our simplifying assumptions.

If our results are confirmed, they could also be relevant for the mass distributions of NSs and black holes (BHs). Earlier explosions due to FFCs can lower the minimum NS mass expected from stellar collapse and might help to explain the formation of NSs below $1.2M_{\odot}$, whose observation challenges current CCSN models [38,61]. For example, our model $M11.2\text{-}2\text{D}\text{-}1e10$ produces a NS with a baryonic mass of only $1.30M_{\odot}$ (gravitational mass of $\sim 1.19M_{\odot}$ for 12 km radius; [62]) instead of $\sim 1.36M_{\odot}$ without FFC. On the other hand, more difficult explosions for massive progenitors would not only raise the BH formation rate, but could also bear on the red supergiant problem, i.e., the lack of observed type-II SNe from progenitors with zero-age-main-sequence masses above $17\text{--}20M_{\odot}$ [63], although current 2D and 3D models yield explosions well beyond this mass range [8,64].

J. E. is grateful to Robert Glas and Oliver Just for their introduction to the use of the ALCAR code. This work was supported by the German Research Foundation (DFG) through the Collaborative Research Centre “Neutrinos and Dark Matter in Astro- and Particle Physics (NDM),” Grant No. SFB-1258-283604770, and under Germany’s Excellence Strategy through the Cluster of Excellence ORIGINS EXC-2094-390783311. In Copenhagen this project received funding from the Villum Foundation (Project No. 37358) and the Danmarks Frie Forskningsfonds (Project No. 8049-00038B). S. A., G. R., and H. T. J. would like to express special thanks to the Mainz Institute for Theoretical Physics (MITP) of the Cluster of Excellence PRISMA+ (Project ID 39083149), for its hospitality and its partial support during the completion of this work. We also acknowledge the use of the following software: MATPLOTLIB [65], NumPy [66], SciPy [67], and IPython [68].

-
- [1] H.-T. Janka, Explosion mechanisms of core-collapse supernovae, *Annu. Rev. Nucl. Part. Sci.* **62**, 407 (2012).
 - [2] H.-T. Janka, T. Melson, and A. Summa, Physics of core-collapse supernovae in three dimensions: A sneak preview, *Annu. Rev. Nucl. Part. Sci.* **66**, 341 (2016).
 - [3] B. Müller, The status of multidimensional core-collapse supernova models, *Pub. Astron. Soc. Aust.* **33**, e048 (2016).
 - [4] H.-T. Janka, Neutrino-driven explosions, in *Handbook of Supernovae*, edited by A.W. Alsabti and P. Murdin (Springer, New York, 2017), p. 1095, [10.1007/978-3-319-21846-5_109](https://doi.org/10.1007/978-3-319-21846-5_109).

- [5] B. Müller, Hydrodynamics of core-collapse supernovae and their progenitors, *Living Rev. Comput. Astrophys.* **6**, 3 (2020).
- [6] A. Burrows, D. Radice, D. Vartanyan, H. Nagakura, M. A. Skinner, and J. C. Dolence, The overarching framework of core-collapse supernova explosions as revealed by 3D FORNAX simulations, *Mon. Not. R. Astron. Soc.* **491**, 2715 (2020).
- [7] A. Mezzacappa, E. Endeve, O. E. B. Messer, and S. W. Bruenn, Physical, numerical, and computational challenges of modeling neutrino transport in core-collapse supernovae, *Living Rev. Comput. Astrophys.* **6**, 4 (2020).
- [8] A. Burrows and D. Vartanyan, Core-collapse supernova explosion theory, *Nature (London)* **589**, 29 (2021).
- [9] S. A. Colgate and R. H. White, The hydrodynamic behavior of supernovae explosions, *Astrophys. J.* **143**, 626 (1966).
- [10] H. A. Bethe and J. R. Wilson, Revival of a stalled supernova shock by neutrino heating, *Astrophys. J.* **295**, 14 (1985).
- [11] H. Duan, G. M. Fuller, and Y.-Z. Qian, Collective neutrino oscillations, *Annu. Rev. Nucl. Part. Sci.* **60**, 569 (2010).
- [12] A. Mirizzi, I. Tamborra, H.-T. Janka, N. Saviano, K. Scholberg, R. Bollig, L. Hüdepohl, and S. Chakraborty, Supernova neutrinos: Production, oscillations and detection, *Riv. Nuovo Cimento* **39**, 1 (2016).
- [13] I. Tamborra and S. Shalgar, New developments in flavor evolution of a dense neutrino gas, *Annu. Rev. Nucl. Part. Sci.* **71**, 165 (2021).
- [14] S. Richers and M. Sen, Fast flavor transformations, in *Handbook of Nuclear Physics*, edited by I. Tanihata, H. Toki, and T. Kajino (Springer Nature, Singapore, 2022), 10.1007/978-981-15-8818-1_125-1.
- [15] M. C. Volpe, Neutrinos from dense: Flavor mechanisms, theoretical approaches, observations, new directions, arXiv:2301.11814.
- [16] J. Pantaleone, Neutrino oscillations at high densities, *Phys. Lett. B* **287**, 128 (1992).
- [17] R. F. Sawyer, Speed-up of neutrino transformations in a supernova environment, *Phys. Rev. D* **72**, 045003 (2005).
- [18] R. F. Sawyer, Multiangle instability in dense neutrino systems, *Phys. Rev. D* **79**, 105003 (2009).
- [19] R. F. Sawyer, Neutrino Cloud Instabilities Just above the Neutrino Sphere of a Supernova, *Phys. Rev. Lett.* **116**, 081101 (2016).
- [20] I. Izaguirre, G. Raffelt, and I. Tamborra, Fast Pairwise Conversion of Supernova Neutrinos: A Dispersion-Relation Approach, *Phys. Rev. Lett.* **118**, 021101 (2017).
- [21] S. Chakraborty, R. S. Hansen, I. Izaguirre, and G. Raffelt, Self-induced neutrino flavor conversion without flavor mixing, *J. Cosmol. Astropart. Phys.* **03** (2016) 042.
- [22] T. Morinaga, Fast neutrino flavor instability and neutrino flavor lepton number crossings, *Phys. Rev. D* **105**, L101301 (2022).
- [23] T. Morinaga, H. Nagakura, C. Kato, and S. Yamada, Fast neutrino-flavor conversion in the preshock region of core-collapse supernovae, *Phys. Rev. Res.* **2**, 012046(R) (2020).
- [24] S. Abbar, F. Capozzi, R. Glas, H.-T. Janka, and I. Tamborra, On the characteristics of fast neutrino flavor instabilities in three-dimensional core-collapse supernova models, *Phys. Rev. D* **103**, 063033 (2021).
- [25] R. Glas, H.-T. Janka, F. Capozzi, M. Sen, B. Dasgupta, A. Mirizzi, and G. Sigl, Fast neutrino flavor instability in the neutron-star convection layer of three-dimensional supernova models, *Phys. Rev. D* **101**, 063001 (2020).
- [26] H. Nagakura, L. Johns, A. Burrows, and G. M. Fuller, Where, when, and why: Occurrence of fast-pairwise collective neutrino oscillation in three-dimensional core-collapse supernova models, *Phys. Rev. D* **104**, 083025 (2021).
- [27] F. Capozzi, S. Abbar, R. Bollig, and H.-T. Janka, Fast neutrino flavor conversions in one-dimensional core-collapse supernova models with and without muon creation, *Phys. Rev. D* **103**, 063013 (2021).
- [28] S. Abbar, H. Duan, K. Sumiyoshi, T. Takiwaki, and M. C. Volpe, On the occurrence of fast neutrino flavor conversions in multidimensional supernova models, *Phys. Rev. D* **100**, 043004 (2019).
- [29] J. Ehring, S. Abbar, H.-T. Janka, and G. Raffelt, Fast neutrino flavor conversion in core-collapse supernovae: A parametric study in 1D models, *Phys. Rev. D* **107**, 103034 (2023).
- [30] O. Just, M. Obergaulinger, and H.-T. Janka, A new multidimensional, energy-dependent two-moment transport code for neutrino-hydrodynamics, *Mon. Not. R. Astron. Soc.* **453**, 3386 (2015).
- [31] O. Just, R. Bollig, H.-T. Janka, M. Obergaulinger, R. Glas, and S. Nagataki, Core-collapse supernova simulations in one and two dimensions: comparison of codes and approximations, *Mon. Not. R. Astron. Soc.* **481**, 4786 (2018).
- [32] M. Zaizen and H. Nagakura, Characterizing quasi-steady states of fast neutrino-flavor conversion by stability and conservation laws, *Phys. Rev. D* **107**, 123021 (2023).
- [33] S. E. Woosley and A. Heger, Nucleosynthesis and remnants in massive stars of solar metallicity, *Phys. Rep.* **442**, 269 (2007).
- [34] S. E. Woosley and A. Heger, The remarkable deaths of 9-11 solar mass stars, *Astrophys. J.* **810**, 34 (2015).
- [35] S. E. Woosley, A. Heger, and T. A. Weaver, The evolution and explosion of massive stars, *Rev. Mod. Phys.* **74**, 1015 (2002).
- [36] D. Radice, A. Burrows, D. Vartanyan, M. A. Skinner, and J. C. Dolence, Electron-capture and low-mass iron-core-collapse supernovae: New neutrino-radiation-hydrodynamics simulations, *Astrophys. J.* **850**, 43 (2017).
- [37] R. Glas, O. Just, H.-T. Janka, and M. Obergaulinger, Three-dimensional core-collapse supernova simulations with multidimensional neutrino transport compared to the ray-by-ray-plus approximation, *Astrophys. J.* **873**, 45 (2019).
- [38] G. Stockinger, H.-T. Janka, D. Kresse, T. Melson, T. Ertl, M. Gabler, A. Gessner, A. Wongwathanarat, A. Tolstov, S. C. Leung, K. Nomoto, and A. Heger, Three-dimensional models of core-collapse supernovae from low-mass progenitors with implications for crab, *Mon. Not. R. Astron. Soc.* **496**, 2039 (2020).
- [39] R. Buras, H.-T. Janka, M. Rampp, and K. Kifonidis, Two-dimensional hydrodynamic core-collapse supernova simulations with spectral neutrino transport. II. Models for different progenitor stars, *Astron. Astrophys.* **457**, 281 (2006).

- [40] A. Marek and H.-T. Janka, Delayed neutrino-driven supernova explosions aided by the standing accretion-shock instability, *Astrophys. J.* **694**, 664 (2009).
- [41] T. Takiwaki, K. Kotake, and Y. Suwa, Three-dimensional hydrodynamic core-collapse supernova simulations for an $11.2M_{\odot}$ star with spectral neutrino transport, *Astrophys. J.* **749**, 98 (2012).
- [42] B. Müller, The dynamics of neutrino-driven supernova explosions after shock revival in 2D and 3D, *Mon. Not. R. Astron. Soc.* **453**, 287 (2015).
- [43] T. Melson, H.-T. Janka, R. Bollig, F. Hanke, A. Marek, and B. Müller, Neutrino-driven explosion of a 20 solar-mass star in three dimensions enabled by strange-quark contributions to neutrino-nucleon scattering, *Astrophys. J. Lett.* **808**, L42 (2015).
- [44] D. Vartanyan, A. Burrows, D. Radice, M. A. Skinner, and J. Dolence, Revival of the fittest: Exploding core-collapse supernovae from 12 to $25M_{\odot}$, *Mon. Not. R. Astron. Soc.* **477**, 3091 (2018).
- [45] E. O'Connor and C. D. Ott, Black hole formation in failing core-collapse supernovae, *Astrophys. J.* **730**, 70 (2011).
- [46] B. Müller, T. Melson, A. Heger, and H.-T. Janka, Supernova simulations from a 3D progenitor model—Impact of perturbations and evolution of explosion properties, *Mon. Not. R. Astron. Soc.* **472**, 491 (2017).
- [47] R. Bollig, N. Yadav, D. Kresse, H.-T. Janka, B. Müller, and A. Heger, Self-consistent 3D supernova models from -7 minutes to $+7$ s: A 1-Bethe explosion of a $19M_{\odot}$ progenitor, *Astrophys. J.* **915**, 28 (2021).
- [48] R. Bollig, H.-T. Janka, A. Lohs, G. Martínez-Pinedo, C. J. Horowitz, and T. Melson, Muon Creation in Supernova Matter Facilitates Neutrino-Driven Explosions, *Phys. Rev. Lett.* **119**, 242702 (2017).
- [49] C. J. Horowitz, O. L. Caballero, Z. Lin, E. O'Connor, and A. Schwenk, Neutrino-nucleon scattering in supernova matter from the virial expansion, *Phys. Rev. C* **95**, 025801 (2017).
- [50] A. S. Schneider, L. F. Roberts, C. D. Ott, and E. O'Connor, Equation of state effects in the core collapse of a $20M_{\odot}$ star, *Phys. Rev. C* **100**, 055802 (2019).
- [51] H. Yasin, S. Schäfer, A. Arcones, and A. Schwenk, Equation of State Effects in Core-Collapse Supernovae, *Phys. Rev. Lett.* **124**, 092701 (2020).
- [52] M. Obergaulinger, H.-T. Janka, and M. A. Aloy, Magnetic field amplification and magnetically supported explosions of collapsing, non-rotating stellar cores, *Mon. Not. R. Astron. Soc.* **445**, 3169 (2014).
- [53] B. Müller and V. Varma, A 3D simulation of a neutrino-driven supernova explosion aided by convection and magnetic fields, *Mon. Not. R. Astron. Soc.* **498**, L109 (2020).
- [54] J. Matsumoto, Y. Asahina, T. Takiwaki, K. Kotake, and H. R. Takahashi, Magnetic support for neutrino-driven explosion of 3D non-rotating core-collapse supernova models, *Mon. Not. R. Astron. Soc.* **516**, 1752 (2022).
- [55] V. Varma, B. Müller, and F. R. N. Schneider, 3D simulations of strongly magnetized non-rotating supernovae: Explosion dynamics and remnant properties, *Mon. Not. R. Astron. Soc.* **518**, 3622 (2023).
- [56] T. Fischer, N.-U. F. Bastian, M.-R. Wu, P. Baklanov, E. Sorokina, S. Blinnikov, S. Typel, T. Klähn, and D. B. Blaschke, Quark deconfinement as a supernova explosion engine for massive blue supergiant stars, *Nat. Astron.* **2**, 980 (2018).
- [57] T. Rembiasz, M. Obergaulinger, M. Masip, M. A. Pérez-García, M. A. Aloy, and C. Albertus, Heavy sterile neutrinos in stellar core-collapse, *Phys. Rev. D* **98**, 103010 (2018).
- [58] K. Mori, T. Takiwaki, K. Kotake, and S. Horiuchi, Shock revival in core-collapse supernovae assisted by heavy axionlike particles, *Phys. Rev. D* **105**, 063009 (2022).
- [59] T. Kuroda and M. Shibata, Spontaneous scalarization as a new core-collapse supernova mechanism and its multimessenger signals, *Phys. Rev. D* **107**, 103025 (2023).
- [60] H. Nagakura, Roles of Fast Neutrino-Flavor Conversion on the Neutrino-Heating Mechanism of Core-Collapse Supernova, *Phys. Rev. Lett.* **130**, 211401 (2023).
- [61] Y. Suwa, T. Yoshida, M. Shibata, H. Umeda, and K. Takahashi, On the minimum mass of neutron stars, *Mon. Not. R. Astron. Soc.* **481**, 3305 (2018).
- [62] J. M. Lattimer and M. Prakash, Neutron star structure and the equation of state, *Astrophys. J.* **550**, 426 (2001).
- [63] S. J. Smartt, J. J. Eldridge, R. M. Crockett, and J. R. Maund, The death of massive stars—I. Observational constraints on the progenitors of Type II-P supernovae, *Mon. Not. R. Astron. Soc.* **395**, 1409 (2009).
- [64] K. Nakamura, T. Takiwaki, T. Kuroda, and K. Kotake, Systematic features of axisymmetric neutrino-driven core-collapse supernova models in multiple progenitors, *Publ. Astron. Soc. Jpn.* **67**, 107 (2015).
- [65] J. D. Hunter, MATPLOTLIB: A 2D graphics environment, *Comput. Sci. Eng.* **9**, 90 (2007).
- [66] C. R. Harris *et al.*, Array programming with NumPy, *Nature (London)* **585**, 357 (2020).
- [67] P. Virtanen *et al.* (SciPy 1.0 Contributors), SciPy 1.0: Fundamental algorithms for scientific computing in Python, *Nat. Methods* **17**, 261 (2020).
- [68] F. Pérez and B. E. Granger, IPython: A system for interactive scientific computing, *Comput. Sci. Eng.* **9**, 21 (2007).